REGULAR ARTICLE

blood advances

Advancing precision therapy in pediatric acute myeloid leukemia through PDX models and mitochondrial targeting

Ambra Da Ros,[1] Alberto Peloso,[1] Giorgia Longo,[1] Maddalena Benetton,[1] Valentina Indio,[2] Stefano Cairo,[3,4] Monica Sandri,[5] Barbara Buldini,[1,4] Silvia Bresolin,[4] Antonio Rosato,[6,7] Andrea Pession,[2] Claudia Tregnago,[1,4] Franco Locatelli,[8] and Martina Pigazzi[1,4]

[1]Division of Pediatric Hematology, Oncology and Stem Cell Transplant, Department of Women's and Children's Health, University of Padua, Padua, Italy; [2]Pediatric Unit, IRCCS Azienda Ospedaliero-Universitaria di Bologna, Bologna, Italy; [3]Champions Oncology, Rockville, MD; [4]Fondazione Istituto Ricerca Pediatrica Città della Speranza, Padua, Italy; [5]Istituto di Scienza, Tecnologia e Sostenibilità per lo Sviluppo dei Materiali Ceramici, Consiglio Nazionale delle Ricerche, Faenza, Italy; [6]Immunology and Molecular Oncology Unit, Veneto Institute of Oncology, IRCCS, Padova, Italy; [7]Department of Surgery, Oncology and Gastroenterology, University of Padua, Padua, Italy; and [8]Department of Pediatric Hematology and Oncology, IRCCS, Ospedale Pediatrico Bambino Gesù, Catholic University of the Sacred Heart, Rome, Italy

Key Points

- AML PDXs capture patients' AML diversity, facilitate druggable targets identification and unlock new therapeutic frontiers in pAML.
- IACS-010759 with venetoclax combination effectively reduces AML progression in *KMT2A*-r PDXs, supporting mitochondrial targeting.

In pediatric acute myeloid leukemia (pAML) relapse/refractory (R/R) disease occurs frequently, but underlying mechanisms are unclear and effective second-line therapeutic options remain limited. Although genomic characterization has advanced targeted treatments, their clinical implementation, particularly in the pediatric field, is hindered by toxicities or resistance due to poor correlation between preclinical and clinical studies. The use of more robust preclinical models is crucial for developing effective therapies. We established 26 patient-derived xenografts (PDXs) of pAML representing 14 high-risk genetic subtypes. These PDXs faithfully recapitulated the molecular complexity and heterogeneity of primary AML, and preserved the immunophenotypic, genomic, and transcriptomic profiles. Clonal and transcriptomic dynamics were tracked from patient samples to their matched PDXs, and vulnerabilities that could be exploited as therapeutic targets were identified, facilitating the evaluation of multifaceted therapeutic strategies. We selected druggable variants and aberrantly activated pathways in *KMT2A*-rearranged (*KMT2A*-r) AML and performed an in vitro drug screening of actionable targets exploiting a predictive 3-dimensional coculture model. Promising compounds were tested in vivo in AML PDXs. Among new drugs targeting variants and pathways, we demonstrate that the combination of IACS-010759, a mitochondrial complex I inhibitor, and venetoclax, a B-cell lymphoma 2 inhibitor, reduces AML progression in *KMT2A*-r PDXs modeling both disease onset and relapse. The combination of venetoclax with IACS-010759 with a stromal targeting drug slowed AML progression in a resistant model. Overall, our study highlights the power of AML PDXs as a translational platform for novel targeted therapy identification. Our preclinical results testing venetoclax with IACS-010759 in *KMT2A*-r AML strongly support mitochondrial targeting in this genetic AML subtype.

Submitted 6 August 2025; accepted 21 December 2025; prepublished online on *Blood Advances* First Edition 23 January 2026; final version published online 25 March 2026. https://doi.org/10.1182/bloodadvances.2025018002.

Sequencing data generated during this study are available in the Gene Expression Omnibus repository (accession number GSE268003).

Data are available from the corresponding author, Martina Pigazzi (martina.pigazzi@unipd.it), on request.

The full-text version of this article contains a data supplement.

Introduction

Pediatric acute myeloid leukemia (pAML) is a childhood malignancy characterized by a high degree of genetic heterogeneity. Recent clinical trials have reported an improved overall survival rate, approaching 80%. However, ~30% of patients experience relapse, and 7% develop relapse/refractory (R/R) disease.[1] Post-relapse treatment continues to be critical for survival[2] (<50%) and therapeutic options for R/R cases remain limited, primarily due to cumulative toxicities from previous intensive chemotherapy and stem cell transplantation, as well as to delayed adoption timeline for pediatric oncology compared with adults.[3] Market authorization of targeted and immune therapies has revolutionized salvage treatment for B-lymphoblastic acute leukemia[4,5]; however, approval for pAML lags far behind.[6-8] Consequently, the development and validation of innovative targeted therapies for R/R pAML remains at the forefront of current research efforts.

Specific pAML subtypes associated with elevated relapse risk, such as *KMT2A* rearrangements, or mediating resistant disease (such as *NUP98* rearrangements and *CBFA2T3*::*GLIS2* fusion) have been subjected to extensive molecular and functional characterization,[9-12] with the aim to discover alternative therapeutic targets and improve outcomes of patients with pAML. Particularly, *KMT2A*-rearrangments represents the most prevalent genetic aberration in pAML (>20%) with prognostic implications varying based on the specific fusion partner gene involved. Extensive molecular and biological characterization of *KMT2A*-r AML has been performed[13] and, in the last decade, the development of menin inhibitors addressing *HOX* genes overexpression, a consequence of *MEN1-KMT2A* complex formation,[14] changed their second-line treatment. Menin inhibitors represent the paradigm of molecularly targeted therapy for *KMT2A*-r, *NUP98*-r, and *NPM1*-mutated AML,[14] and currently, 18 clinical trials are underway exploring the use of menin inhibitors in the treatment of leukemia. Alongside targeted drugs, the development of antibody-drug conjugates, cellular therapies, and more innovative dual-targeted and adapter chimeric antigen receptor T-cell technologies[15,16] represents a path to further therapeutic approaches with the potential to change the treatment landscape for high-risk adult and pAML.

Overall, the elucidation of molecular dynamics arising from genomic or transcriptomic profiles has generated a growing interest in precision medicine leading to the identification of numerous novel putative therapeutic targets, changing the scenario of what was previously conceived as targetable.[4,17] Since 2017, 12 novel agents have been approved by the US Food and drug Administration for treating different adult AML subsets, including a B-cell lymphoma 2 (BCL-2) inhibitor (venetoclax [VEN]), three Fms-related receptor tyrosine kinase 3 (FLT3) inhibitors, three isocitrate dehydrogenase 1/2 inhibitors, one Hedgehog pathway inhibitor, two oral hypomethylating agents, one anti-CD33 antibody-drug conjugate, and CPX-351.[18] Although these innovative therapeutic strategies have offered tangible treatment opportunities, they have also revealed challenges related to acquired resistance after single-agent regiments.[19-21] The rationale for implementing sequential or alternating multitarget drug regimens is to prevent the onset of resistance while minimizing cytotoxicity and enhancing antineoplastic efficacy.[22] However, a significant hurdle in identifying novel compounds to be translated into effective clinical application lies in the prioritization of relevant actionable vulnerabilities among numerous potential targets. Patient-derived xenograft (PDX) models emerged as feasible tools to simplify targets prioritization process.[23-29]

In line with this, we established and characterized an extensive panel of pAML PDXs to facilitate the identification of unique tumor pathways and subclonal architectures for the development of novel targeted therapeutic strategies. The study of pAML evolution in AML PDXs captures fixed stages of leukemia progression, enabling the PDX models to provide novel validated interventional options for the treatment of high-risk pAML.

Methods

Patient samples

Bone marrow (BM) or peripheral blood (PB) samples of pediatric patients diagnosed with AML other than acute promyelocytic leukemia were provided by the Pediatric Oncohematology BioBank at the pediatric Onco-Hematology Laboratory of the Padova University Hospital, reference center for de novo pAML diagnosis, in accordance with ASSOCIAZIONE ITALIANA EMATOLOGIA ONCOLOGIA PEDIATRICA AML 2002/01[30] and 2013/01 trials and the Leucemia non Linfoblastica Acuta working party (Table 1; supplemental Tables 1 and 6).

PDXs establishment

Female NSG mice (NOD.Cg-Prkdc^{scid} Il2rg$^{tm1Wjl/SzJ}$) were subjected to intrvenous (IV), intrafemoral, or intrahepatic inoculation of 1×10^6 CD3-depleted primary pAML cells to generate P0-PDX (conditioned with 1.5 Gy). In fewer cases, a 3-dimensional (3D) scaffold seeded with primary AML was subcutaneously implanted,[33] as detailed in the supplemental Methods. AML engraftment (human CD45 [hCD45] of >5%) was evaluated by hCD45$^+$ cells in animal PB by flow cytometry. Subsequently, 1×10^6 hCD45 cells collected from the BM or spleen of P0-PDX were IV reinjected into successive recipients, generating P1- and P2-PDXs.

PDXs treatment

A total of 1×10^6 P2-PDX–derived cells (ex vivo) were IV injected into NSG mice and at engraftment (blasts from 5% to 10% in the PB) were treated with VEN (Sigma, Merck, Darmstadt, Germany) 25 mg/kg, IACS-010759 (IACS; Selleckchem, Houston, TX) 7.5 mg/kg, lercanidipine (Sigma, Merck) 1.5 mg/kg, or with cytarabine (Selleckchem) 50 mg/kg plus doxorubicin (Sigma, Merck) 1.5 mg/kg. Further details are reported in the supplemental Methods. Procedures involving animals were in accordance with institutional guidelines that comply with national and international laws and policies and with "ARRIVE" (animal research: reporting of in vivo experiments) guidelines. All animal procedures were authorized by Italian Ministry of Health: 622/2017-PR and 512/2019-PR.

Statistical analyses

Statistical significance of differences in means between 2 groups was evaluated by applying the Student *t* test, after a preliminary testing of normal distribution of data, and the Welch correction was used when needed. Statistical significance of differences in the median between 2 groups was evaluated by applying the

Table 1. Patient and sample characteristics of AML cases used for PDXs generation

	With engraftment	Without engraftment	*P* value (χ^2 test)
No. of patient samples at diagnosis	22	34	
Sex			ns
Male	13	20	
Female	9	14	
Age (y)			.05
0-1	1	1	
1-10	14	11	
10-18	7	22	
WBC (x 10^9/L , average), n = 48	111.13	70.74	ns
Karyotype, n = 27			ns
Complex	3	4	
Genetics			ns
Favorable risk			ns
*NPM1**	0	1	
inv16 (*CBFB*::*MHY11*)	2	1	
+*KIT**	2	0	
t(8;21) *RUNX1*::*RUNX1T1*	0	2	
+*KIT**	1	1	
High risk			.022
t(16;21) *FUS*::*ERG*	1	1	
t(9;11) *KMT2A*::*MLLT3*	5	0	
t(11;19) *KMT2A*::*ENL*	1	1	
*FLT3*ITD	0	4	
*FLT3*ITD+*NPM1**	1	2	
t(16;16) *CBFA2T3*::*GLIS2*	0	1	
t(5;11) *NUP98*::*NSD1*	0	1	
t(5;11) *NUP98*::*NSD1*+*FLT3*ITD	2	1	
*KMT2A*PTD+*FLT3*ITD	0	1	
t(6;11) *KMT2A*::*AFDN*	2	3	
t(10;11) *KMT2A*::*MLLT10*	2	3	
t(3;5) *NPM1*::*MLF1*+*FLT3*ITD	1	0	
t(4;11) *KMT2A*::*AFF1*	1	0	
t(11;12) *NUP98*::*KDM5A*	1	0	
No marker	0	11	
Status			ns
Alive	15	29	
Died	7	5	
Event			.0014
No events	9	28	
Relapse/death	13	6	
Molecular MRD[31] at the end of second induction course, n = 31			ns
$>10^{-3}$	6	7	
$<10^{-3}$	7	11	
Flow MRD[32] at the end of second induction course, n = 44			ns
$>10^{-3}$	4	5	
$<10^{-3}$	11	24	

Engraftment was defined as the presence of >5% hCD45$^+$ cells in P0-PDX PB. Complex karyotype is considered as ≥3 unrelated cytogenetic aberrations. A *P* value > .5 was considered ns.

Flow MRD, minimal residual disease measured by flow cytometry; Molecular MRD, minimal residual disease measured by quantitative polymerase chain reaction; ns, not significant; WBC, white blood cells.

Mann-Whitney *U* test. Analysis of variance test was performed when comparing >2 groups. In PDXs treatment experiment, overall survival was calculated from the date of engraftment (blasts count from 5% to 10% in the PB, that coincides with the first treatment dose) to the time of death (humane end point). To assess the event-free survival of patients whose samples were used to generate PDX models we used the date of diagnosis to the last follow-up or first event (relapse, death in remission, secondary malignancies, whichever occurred first). For survival analyses, we used the Kaplan-Meier method and log-rank test. Correlation analyses were performed using the Pearson method. Graphs and statistical analyses were generated using the GraphPad Prism 8 (GraphPad, La Jolla, CA). All data are presented as mean ± standard error of the mean. Differences were considered statistically significant when the *P* value was <.05 (*), <.01 (**), <.001 (***), or <.0001 (****).

Results

pAML PDXs establishment

We generated a large panel of 26 AML PDX models through serial xenotransplantation of primary cells derived from patients with pAML at diagnosis and/or relapse (supplemental Table 1). The process involved 3 successive murine passages (P0, P1, P2-PDX) and different inoculation methodologies (Figure 1A) to overcome the recognized engraftment difficulties associated with AML.[34] We obtained primary AML cell engraftment (defined as >5% hCD45$^+$ cells in the PB) in P0-PDXs for 26 of 64 (41%) inoculated samples (representative plots of hCD45$^+$-cell monitoring by flow cytometry in supplemental Figure 1A-B). We observed a significantly higher AML engraftment success rate in P0-PDX by IV injection with respect to scaffold implant and intrahepatic or intrafemoral injection (χ^2 test $P = .019$; supplemental Table 2). Therefore, we used the IV method to generate P1- and P2-PDX. By analyzing characteristics of patients with pAML, we found different factors associated with successful engraftment: particularly, pAML harboring a high-risk genetic features, as well as pAML from patients with a poor event-free survival or lower age at diagnosis, significantly improved engraftment success ($P = .022$, $P = .0014$, and $P = .05$ respectively; Table 1; Figure 1B). Overall, we obtained 26 P0-PDX models with different genetic backgrounds (Figure 1C). Interestingly, pAML

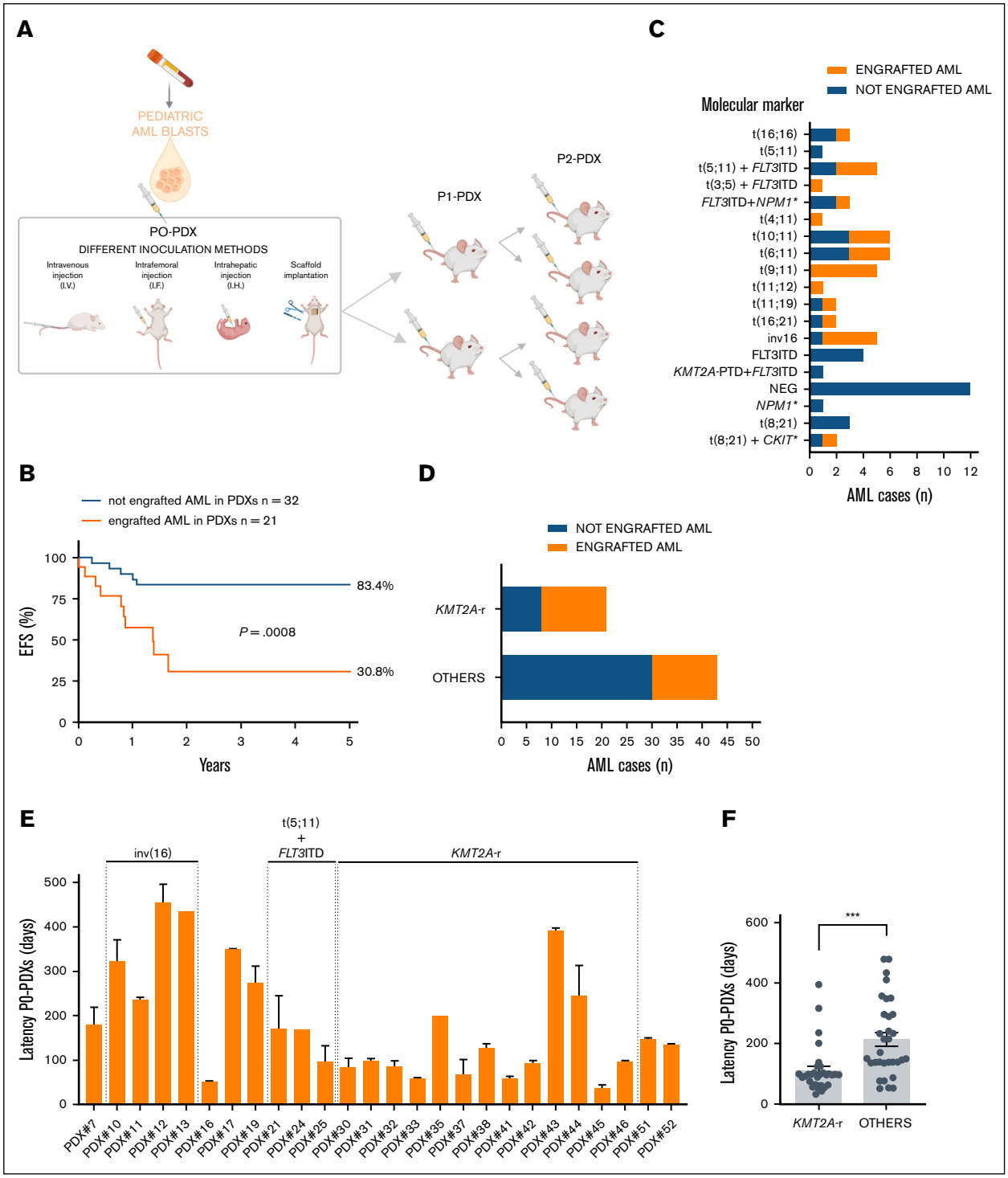

Figure 1. AML PDXs establishment: engraftment, latency, and correlation with patient outcome. (A) Representative workflow for AML PDX generation, from patient AML cell inoculation to successive PDX passages (P0-P1-P2). (B) Kaplan-Meier curve showing 5-year EFS of patients with AML, according to their engraftment in mice; EFS of 30.8% vs 83.4%, respectively; $P = .0008$. (C) Histogram representative of the number of engrafted AML samples in P0-PDX, according to genetic rearrangement. (D) Histogram representative of the number of engrafted *KMT2A*-r samples (n = 13/21) compared with samples characterized by other genetic lesions (n = 13/43); P value = .01. In panels C-D, engrafted samples (defined by the presence of >5% hCD45$^+$ cells in the PB of P0-PDXs) are reported in orange, whereas not-engrafted samples are in blue. (E) Latency (time from primary AML cell inoculation to mouse euthanasia) in P0-PDXs. (F) Average disease latency in P0-PDXs according to different genetic, *KMT2A*-r PDXs (mice, n = 31) compared with other genetically altered PDXs (mice, n = 32). All data are presented as mean ± standard error of the mean (SEM). ****$P < .0001$. EFS, event-free survival.

harboring *KMT2A*-rearrangments were highly represented (n = 13/26; Figure 1C-D; supplemental Table 3). Latency (defined as time from mouse inoculation to euthanasia) of P0-PDXs was extremely heterogeneous, with a median time of 135 days (Figure 1E; supplemental Table 3); samples that successfully engrafted in secondary (P1) and tertiary (P2) recipients showed heterogeneous but reduced latency (supplemental Figure 1C), with a median of 90 days from P1- to P2-PDXs (supplemental Figure 1D). Furthermore, the proportion of $hCD45^+$ cells in mouse PB increased more rapidly during the second and third passages compared with the initial passage from PT-AML to P0-PDX (supplemental Figure 1E). Noteworthy, samples with genetic profiles associated to a favorable risk, such as inv(16) *CBFB*::*MYH11*, showed a long latency (Figure 1E); on the contrary, *KMT2A*-r AML showed a faster engraftment, when compared with other genetic subtypes of pAML (110 ± 14 days vs 213 ± 22 days, respectively; $P = .0003$; Figure 1F).

AML PDXs reveal AML clonal dynamics

Throughout sequential PDX passages, we conducted comprehensive analyses of AML immunophenotype, genomic profile, and transcriptomic landscape to evaluate the fidelity of these models to the original patient-AML. Immunophenotypic profile revealed an overall concordance among primary PT-AML and paired PDXs, with no evidence of enrichment or depletion of peculiar subpopulations (n = 8 matched samples; supplemental Table 4; supplemental Figure 2A). By whole-exome sequencing we showed that variants detected in PT-AML samples were consistently maintained in the P2-PDXs (a total of 179 maintained variants of 184 found [97.3%]; n = 8 matched samples), indicating a strong genomic similarity between human AML and the AML propagated in mice (Figure 2; supplemental Table 5). Briefly, most mutations were missense single-nucleotide variants, whereas we observed a low number of frameshift/nonframeshift insertions/deletions. Among known AML-driver genes, we identified *NRAS*, *CREBBP*, *FAT1*, *TET2*, *FLT3*, *NOTCH1*, and *KDM5A* as the most frequently mutated genes (from 25% to 38%), regardless of the presence of co-occurring genetic aberrations (Figure 2B). Across all pairs, most variants were preserved in P2-PDX, whereas a minority of variants were lost or gained in the PDX. By using variant allele frequency (VAF) we inferred the clonal architecture of patient-AML and of the matched PDX. A lower VAF correlation between patient-AML and matched P2-PDX (Pearson correlation coefficient, 0.42; Figure 3A; supplemental Figure 2B) was found with respect to intra-PDXs VAF correlation (P0-P2; Pearson correlation coefficient, 0.91; Figure 3B). We documented an average of 22 variants per sample (range, 13-42) and we showed that the AML PDX models preserved the patient-AML founder clone, defined at least by 1 variant affecting an AML driver gene[35] and other variants with a VAF of 50% (Figure 3A; supplemental Figure 2B). Variants of uncertain significance in other genes were also detected and, notably, we identified 6 mutated genes (*NCOR1*, *CCND3*, *AXIN1*, *AFF3*, *ARID1A*, and *FAT1*) that were previously reported as mutated in another AML cohorts,[17] supporting their further characterization as possible recurrent pAML mutations (supplemental Table 5). Considering the cancer cell fraction from patient-AML to P2-PDX, we established 3 different patterns of clone dynamics defined as loss, acquisition, or expansion (Figure 3C). Clone loss involved mutations in *WT1* and *NUP98* in AML19, *KRAS* in AML35, and *SETD2* in AML46. In 4 P2-PDX models we observed the acquisition of clones, particularly characterized by *WT1* mutation in AML17, *CCND3* mutation in AML19, *ARID1A* deletion in AML42, and *FLT3* and *ASXL1* mutations in AML43. In 1 model (AML35) we identified the expansion of a *FLT3*-mutated subclone (Figure 3C). Notably, in most P2-PDX models (7/8) we found variants of uncertain significance acquisition with respect to the original patient-AML. Overall, the inference of the evolutionary clonal trajectories from patients to models informed about the most relevant variants for targeting, and about clones with potential to sustain AML reemergence.

Variants targeting in a 3D model

Genomic targeting represents a therapeutic approach to expand the landscape of potential interventions,[22] therefore we attempted to investigate a possible functional role of genomic lesions identified by whole-exome sequencing using tailored treatments in ex vivo AML PDX–derived cells (n = 4). In detail, we used 5-azacitidine (AZA) to treat clones characterized by cells harboring mutations in epigenetic regulators (such as *KDM5A*, *CREBBP*, *ASXL1*, *TET2*), quizartinib to treat *FLT3ITD* mutated cells, trametinib for cells harboring mutations in genes involved in the RAS-RAF-MEK-ERK pathway, γ-secretase inhibitor X for those with *NOTCH* mutations, and ICG-001 for cells showing variants in genes involved in the regulation of Wnt/β-catenin signaling pathway. Selected drugs were tested on a reliable in vitro setting, using a 3D coculture system that allows a more predictive drug efficacy evaluation. This tool, previously set up and used in our laboratory,[33,36] consists of a biomimetic scaffold made of hydroxyapatite/collagen (70%/30%) in which mesenchymal stromal cells (MSCs)derived from the BM of patients with AML (AML-MSCs) were cocultured with AML blasts. Exploiting this 3D system (workflow in Figure 4A), targeted drugs were tested as single agents or combined with VEN, a BCL-2 inhibitor. Recently VEN has significantly affected the treatment landscape of adult hematological malignancies; however, its efficacy as monotherapy is limited[37] and data on how best to incorporate VEN into treatment remain a critical gap in the field of pAML.[38] In this experimental setting, we combined VEN with the selected compounds to pursue a rational multinode targeting strategy integrating genomic evidences. Interestingly, AML30 (*FAT1* and *AXIN1* variants) and AML35 (*AFF3* mutation) showed a reduction in blast viability after treatment with Inhibitor of CBP/β-Catenin Gene transcription-001 (ICG-001), a CREB-Binding Protein (CBP)/β-catenin inhibitor blocking β-catenin–dependent gene transcription (Figure 4B-C). In addition, results suggested that ICG-001 in combination with VEN significantly impaired AML30 proliferation (Figure 4B). Notably, AML35 showed very low sensitivity to most drugs tested in vitro (Figure 4C). AML43 demonstrated sensitivity to VEN and to quizartinib, suggesting a putative functional impact of the *FLT3* single-nucleotide variants that emerged in the PDX founder clone (Figure 4D). VEN emerged as the most effective drug for AML46, and the combination of VEN with AZA indicated the absence of a synergistic effect in ex vivo cells from this PDX model. (Figure 4E). These data uncovered possibly targetable variants in Wnt/β-catenin signaling in AML.

AML PDXs accurately capture core transcriptional features of AML

Our in vitro studies demonstrated promising results in targeting a specific gene variant; however, the patient-specific nature of novel genomic-tailored approaches present significant challenges for

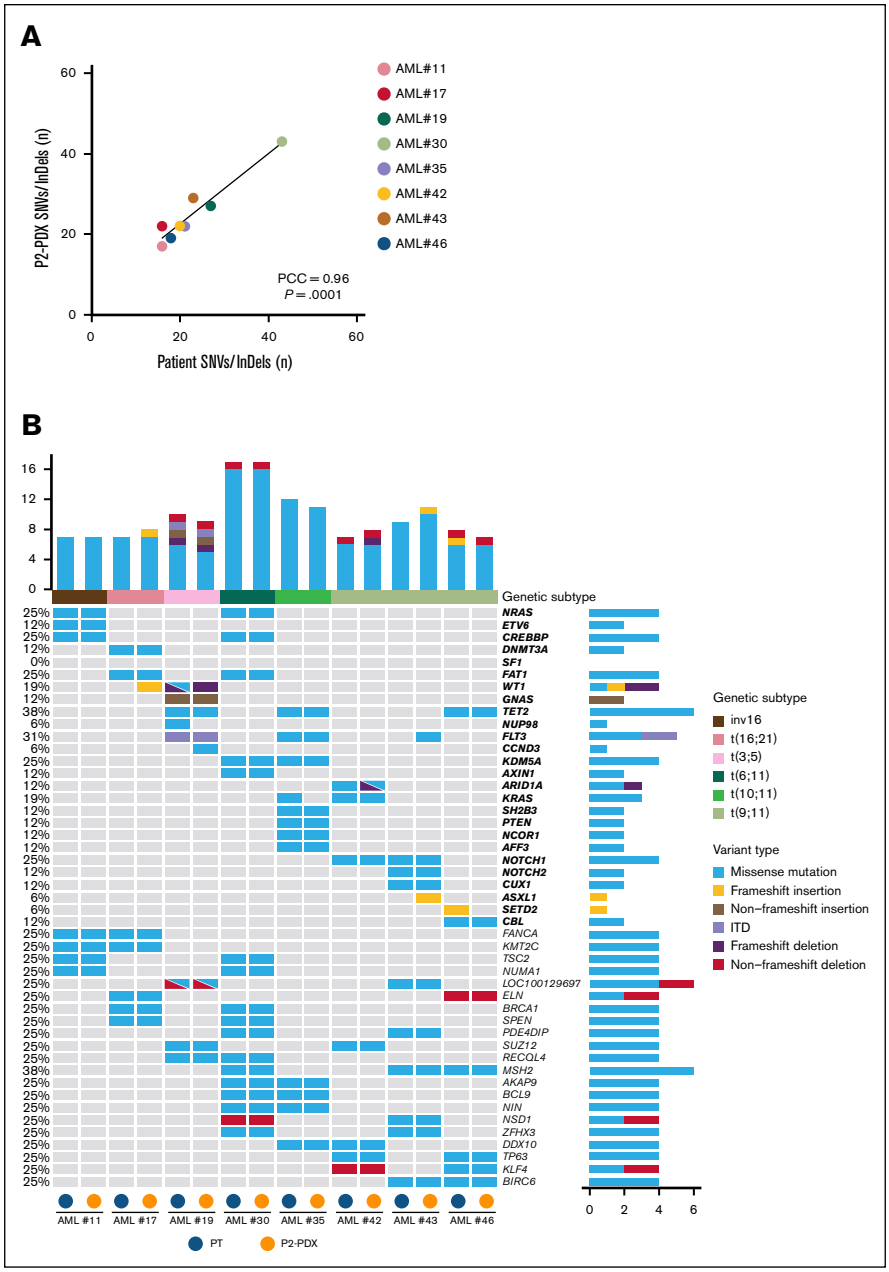

Figure 2. Genomic profiles of AML blasts derived from patients and matched PDXs. (A) Total number (n) of SNVs/InDels detected in PT-AML (x-axis) and in the corresponding P2-PDX (y-axis). PCC of 0.96 ($P < .0001$). (B) Oncoplot representing the AML mutational landscape in our cohort. Each column is relative to a single AML sample; samples are grouped in couples of patient and matched P2-PDX AML; on the lower part of the oncoplot, blue dots indicate patient AML tumor origin, whereas orange dots indicate P2-PDXs. Colors in the oncoplot indicate different mutation types, triangles indicate the mutations co-occurrence. The upper bar plot reports absolute number and type of mutation for each sample; the right bar plot reports the number of samples harboring mutations in each specific gene. On the left of the oncoplot the relative frequency of mutated gene in the entire cohort is indicated. Samples are grouped into defined genetic subtypes. AML driver genes are in bold, whereas recurrently mutated genes (at least in 2/8 AML-coupled samples, PT and P2-PDX) have been reported in regular font. InDels, insertion/deletions; ITD, internal tandem duplication; PCC, Pearson correlation coefficient; PT, patient; SNVs, single-nucleotide variants.

immediate clinical translation. By comparison, pathway-based approaches represent a widely accepted framework for targeted therapy. Therefore, we investigated AML gene expression during the complex process of PDX establishment, with the goal to identify new treatment opportunities.

RNA sequencing confirmed the transcriptional stability of AML across serial PDX passages (from P0 to P3; supplemental Figure 3A), indicating the reproducibility of the model. Notably, gene expression profiles of primary patient-AML samples and their matched PDXs were highly correlated and clustered closely, regardless of patients' genetic background (Figure 5A; supplemental Figure 3B), highlighting the ability of PDX models to faithfully preserve patient-specific leukemic transcriptional programs.

Subsequently, we focused on *KMT2A*-r AML with respect to other AML genetic subtypes, considering its high frequency and the efforts spent to find new drugs for this AML subtype in the last decade.[39,40] By gene set enrichment analysis we found that AML *KMT2A*-r samples from both patients and from PDXs were associated with increased mitochondria-related biological processes and oxidative phosphorylation (OXPHOS; Figure 5B; supplemental Tables 7 and 8). To functionally validate gene set enrichment analysis results, we demonstrated a significantly higher mitochondrial dependence in ex vivo *KMT2A*-r AML cells with respect to AML blasts characterized by other genetics (Figure 5C).

In addition, in a protein analysis of 60 AML samples at diagnosis,[41] we found that *KMT2A*-r AML exhibited significantly higher BCL-2 expression with respect to other AML samples (Figure 5D;

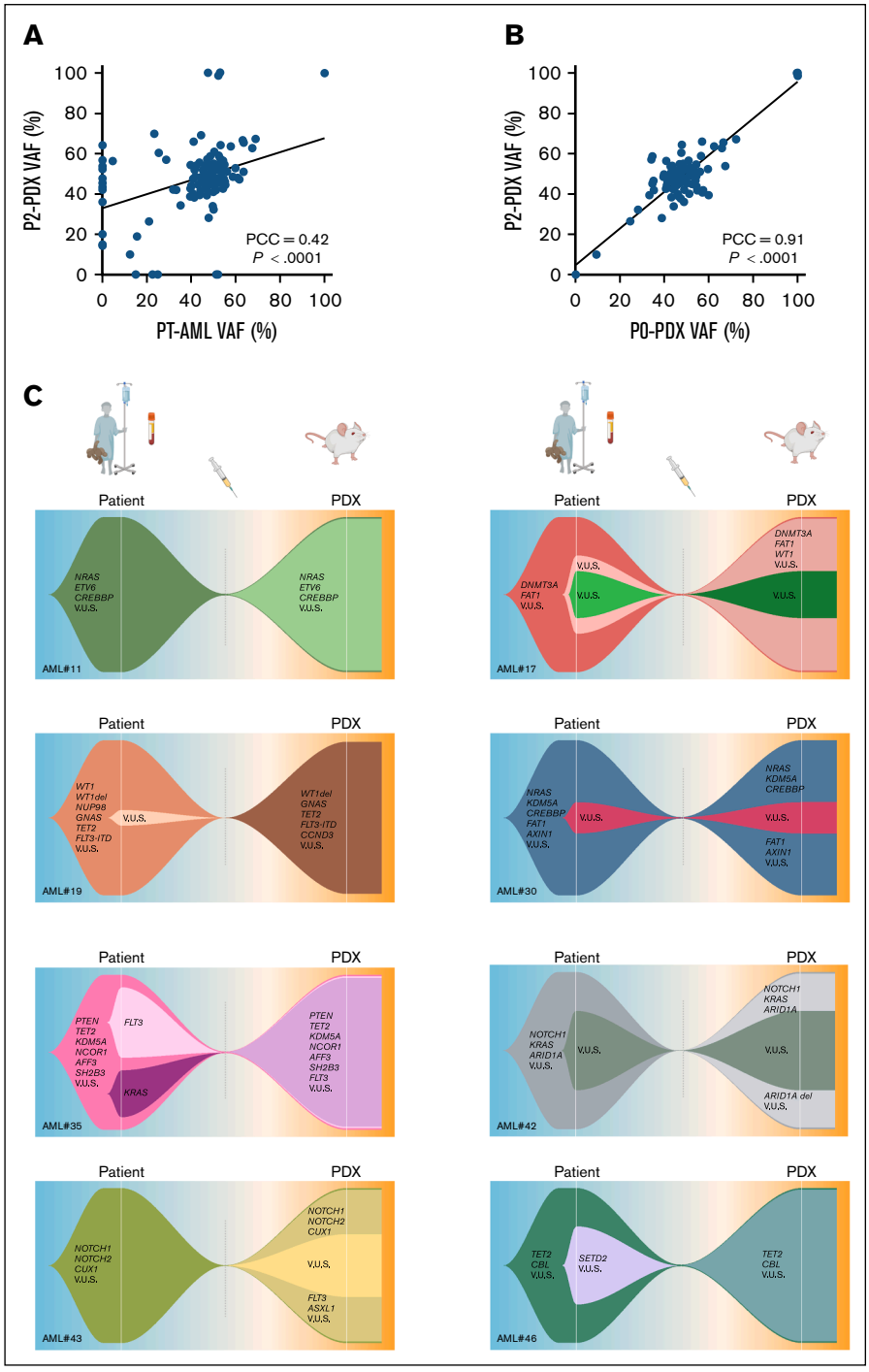

Figure 3. AML clonal evolution from patients to matched PDXs. (A-B) Correlation plot of VAF detected in PT-AML (x-axis) and P2-PDXs (y-axis) (A). PCC of 0.42; *P* value <.0001 and in P0-PDX (x-axis) and in P2-PDX (y-axis) (B). PCC of 0.91; *P* < .0001 (C) Fish plot of AML clonal architecture inferred from the cancer cell fraction (CCF) in PT-AML and in P2-PDXs. CCF-based variant clonal clusters are shown in different colors; same color with a different nuance among PT and P2-PDX indicates that variants, including VUS, are different. The complete list of variants is reported in supplemental Table 5. PCC, Pearson correlation coefficient; PT, patient. VUS, variants of uncertain significance.

supplemental Table 6). We confirmed that *KMT2A*-r blasts derived from PDXs exhibited elevated *BCL-2* expression levels (Figure 5E), reinforcing that AML PDXs faithfully represent patients' AML and enable the prioritization of actionable therapies.

Pharmacological *KMT2A*-r AML targeting in vitro in a 3D model

Emerging evidence from patient-AML and from PDX models indicated that *KMT2A*-r blasts display a marked reliance on

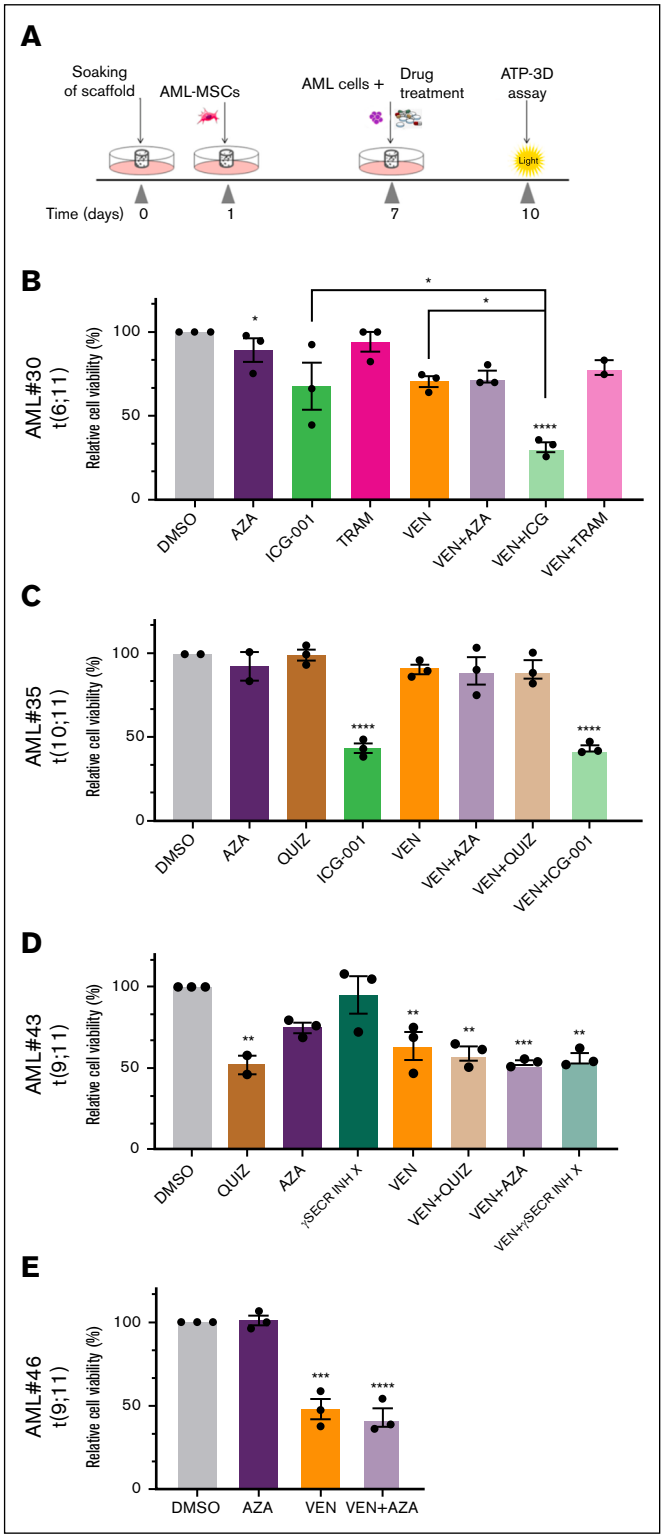

Figure 4. Pharmacological targeting of candidates emerged from genomic data. (A) 3D coculture/treatment workflow: scaffolds were allowed to soak 24 hours before seeding with MSCs (day 1) that remain into the scaffold for 6 days before the addition of ex vivo AML cells and the concomitant drug treatment (day 7). Cell viability of 3D system was evaluated 72 hours after treatments (day 10), by 3D ATP assay. (B-E) Cell viability of 3D system, treated with compounds targeting patient-specific

antiapoptotic signaling, supporting the therapeutic rationale for targeting BCL-2 with VEN.[42,43] Because transcriptomic and functional data highlighted mitochondrial respiration as central in *KMT2A*-r AML biology, we designed a combinatorial approach coupling VEN with a compound recently identified to target mitochondrial respiration in cancer, IACS, an inhibitor of complex I of the mitochondrial electron transport chain, suppressing OXPHOS.[44] By generating dose-response curves of VEN and IACS on ex vivo *KMT2A*-r AML blasts (n = 6; Figure 6A), we revealed a high intersample heterogeneity (50% effective concentration dosage; supplemental Table 9) and moved to a more reliable in vitro testing approach, using the 3D coculture system that we had previously set up and described.[33] We treated scaffolds cocultured with AML-MSCs and ex vivo AML cells with VEN and IACS at patient-specific 50% effective concentration doses, either as single agents or in combination (following the workflow in Figure 4A), ensuring absent toxicity on MSCs alone (supplemental Figure 3C). Selectively in *KMT2A*-r blasts, the combination of VEN with IACS reduced cell viability by >50% and was synergistic with a combination index[45] of 0.62 (Figure 6B), offering new insights for treatment opportunities in this high-risk genetic subgroup.

Preclinical validation of mitochondrial targeting in *KMT2A*-r AML in vivo

In light of our in vitro results, we tested VEN in combination with IACS in 3 different *KMT2A*-r AML PDXs. All PDX models treated with VEN in combination with IACS achieved blast clearance (hCD45 of <5%) at treatment discontinuation, showing improved leukemia eradication with respect to VEN (day 30; Figure 7A) and to IACS as single agents (supplemental Figure 4B), without significant changes in mouse body weight (supplemental Figure 4A). Notably, this response was maintained after treatment discontinuation in 2 of 3 models (PDX31 and PDX43) that showed a lower blasts infiltration in the BM and spleen, confirming the higher efficacy of VEN plus IACS compared with VEN alone (Figure 7B; supplemental Figure 4C). Despite the small group size for the survival studies, mice treated with VEN plus IACS benefited from a significantly prolonged survival, highlighting the superiority of the combination ($P < .01$; Figure 7C; supplemental Figure 4D-E). In particular, we observed, on average, a 39% longer life span (from treatment start), prolonging the median life span by 29 and 57 days (PDX31 and PDX43, respectively), in mice treated with VEN plus IACS with respect to VEN. We also demonstrated the superiority of the combination with respect to a traditional chemotherapeutic agent (cytarabine, Ara-C), used as comparator in PDX31 (Figure 7D-E).

Figure 4 (continued) genomic alterations or with VEN, used as single agents and in combinations. AZA, 2μM; ICG-001, 5μM, TRAM, 5nM; QUIZ, 0.2μM; and γSECR INH X, 10μM. Patient-specific 50% effective concentration (EC_{50}) dosage of VEN was used (patient-specific EC_{50} table reported in supplemental Table 9). Values of cell viability are normalized to respective controls, and treatments were performed in 3 independent replicates. All data are presented as mean ± SEM. *$P < .05$; **$P < .01$; ***$P < .001$; ****$P < .0001$. Statistical significance reported above the bars are relative to DMSO. PCC, Pearson correlation coefficient; DMSO, dimethyl sulfoxide; γSECR INH X, γ-secretase inhibitor X; QUIZ, quizartinib; AZA, Azacytidine; TRAM, trametinib.

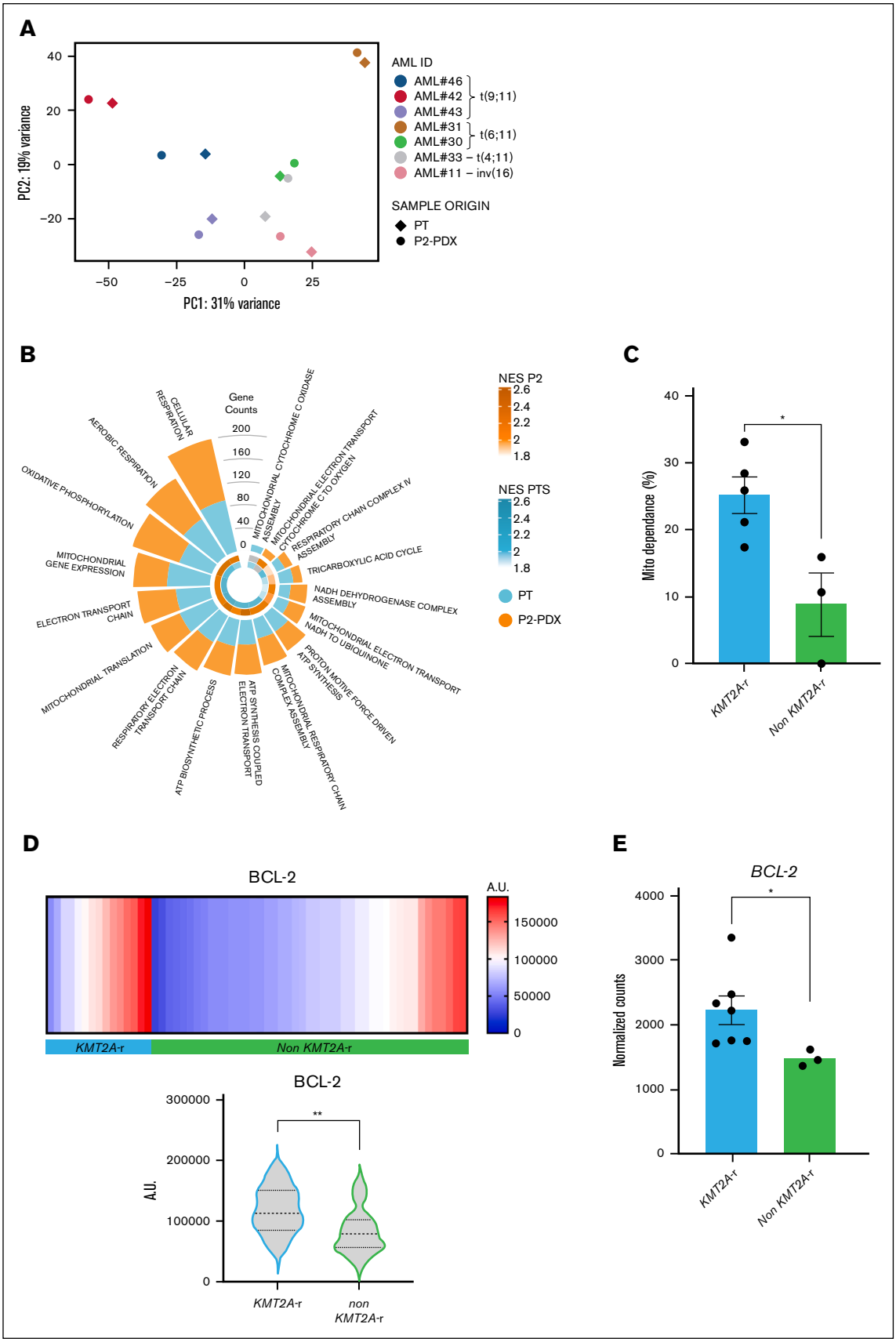
A
PC2: 19% variance
PC1: 31% variance
AML ID
AML#46
AML#42
AML#43
t(9;11)
AML#31
AML#30
t(6;11)
AML#33 – t(4;11)
AML#11 – inv(16)
SAMPLE ORIGIN
PT
P2-PDX
B
Gene Counts
NES P2
NES PTS
PT
P2-PDX
CELLULAR RESPIRATION
AEROBIC RESPIRATION
OXIDATIVE PHOSPHORYLATION
MITOCHONDRIAL GENE EXPRESSION
ELECTRON TRANSPORT CHAIN
MITOCHONDRIAL TRANSLATION
RESPIRATORY ELECTRON TRANSPORT CHAIN
ATP BIOSYNTHETIC PROCESS
ATP SYNTHESIS COUPLED ELECTRON TRANSPORT
MITOCHONDRIAL RESPIRATORY CHAIN COMPLEX ASSEMBLY
PROTON MOTIVE FORCE DRIVEN ATP SYNTHESIS
MITOCHONDRIAL ELECTRON TRANSPORT NADH TO UBIQUINONE
NADH DEHYDROGENASE COMPLEX ASSEMBLY
TRICARBOXYLIC ACID CYCLE
RESPIRATORY CHAIN COMPLEX IV ASSEMBLY
MITOCHONDRIAL ELECTRON TRANSPORT CYTOCHROME C TO OXYGEN
MITOCHONDRIAL CYTOCHROME C OXIDASE ASSEMBLY
C
Mito dependance (%)
KMT2A-r
Non KMT2A-r
D
BCL-2
A.U.
KMT2A-r
Non KMT2A-r
BCL-2
A.U.
KMT2A-r
non KMT2A-r
E
BCL-2
Normalized counts
KMT2A-r
Non KMT2A-r

Figure 5.

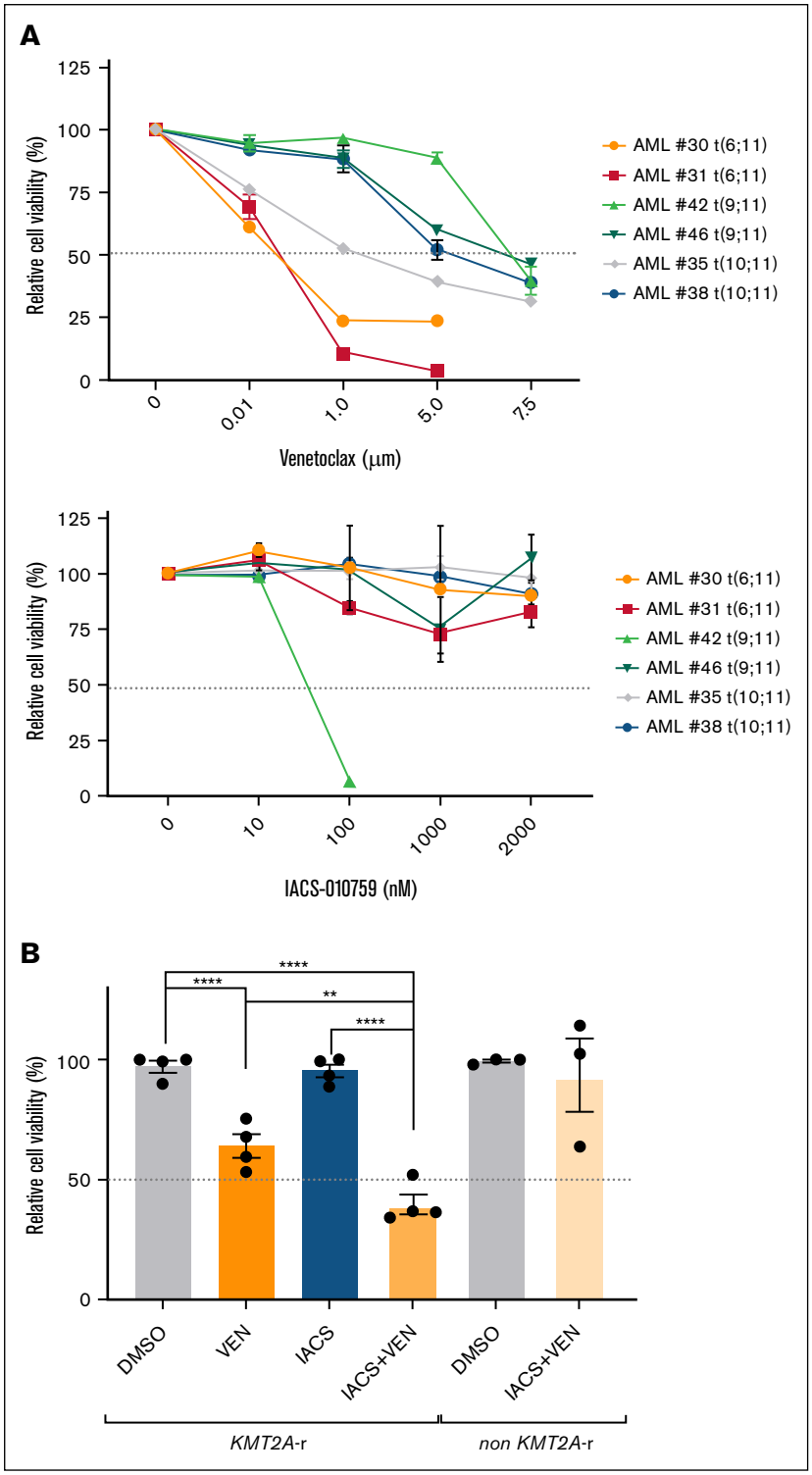

Figure 6. In vitro testing of compounds targeting novel transcriptomic vulnerabilities of AML. (A) Dose response curve performed on 6 different ex vivo AML cells, after 72 hours of treatment with VEN and IACS. Patient-specific EC_{50} values relative to the different compounds are reported in supplemental Table 9. (B) Cell viability of 3D system, with i*KMT2A*-r (left) or non–*KMT2A*-r (right) treated with patient-specific EC_{50} dosage of VEN and IACS, normalized to respective controls (n = 4 *KMT2A*-r and n = 3 non–*KMT2A*-r ex vivo samples). All data are presented as mean ± SEM. $^{**}P < .01$; $^{****}P < .0001$. DMSO, dimethyl sulfoxide.

Figure 5. RNA sequencing of original AML and matched PDXs highlight transcriptomic AML core. (A) Unsupervised principal component analysis of PT-AML and P2-PDX (n = 7 models). Colors are representative of different AML; squares indicate PT-AML, whereas circles show AML PDX. (B) Circular bar pot of selected biological processes related to mitochondria, in *KMT2A*-r samples vs other genetically rearranged AML derived by gene set enrichment analysis. Bar height represents the number of genes enriched in each gene set; in blue, data relative to patient samples (*KMT2A*-r, n = 6; other genetics, n = 3); in orange, data of P2-PDX samples (*KMT2A*-r, n = 7; other genetics, n = 3); central heat map is relative to NES value of enriched process. (C) Mitochondrial dependence of human AML cells derived from *KMT2A*-r (n = 5, blue) and non–*KMT2A*-r (n = 3, green) PDXs, assessed using SCENITH (single-cell energetic metabolism by profiling translation inhibition) methodology by flow cytometry. (D) Expression of antiapoptotic protein BCL-2 in a cohort of 60 patients with pAML subcategorized into *KMT2A*-r (n = 15) and non–*KMT2A*-r AML (n = 45), analyzed with the reverse-phase protein array method. $^{**}P < .01$. (E) Gene expression of *BCL-2* in *KMT2A*-r (n = 7) and non–*KMT2A*-r (n = 3) P2-PDXs. Histogram represents normalized counts. All data are presented as mean ± SEM. $^{*}P < .05$; $^{**}P < .01$. A.U., arbitrary units; Mito, mitochondial; NES, normalized enrichment score; PC1/2, principal component 1/2; PT, patient; PTS, patients.

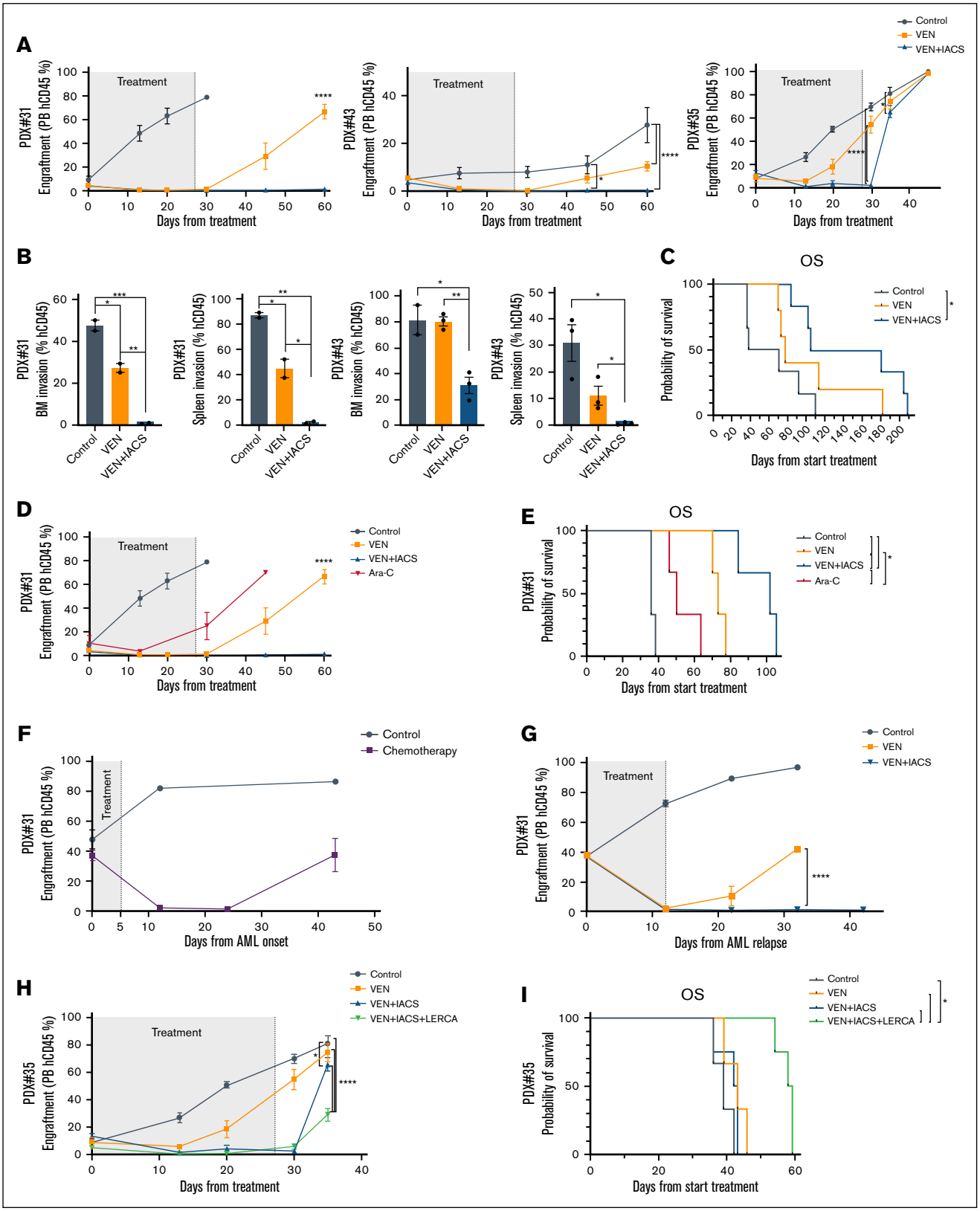

Figure 7. In vivo preclinical testing of novel combinations on AML PDXs. (A) Monitoring of hCD45$^+$ AML cell percentage in the PB of PDXs during treatment with VEN (25 mg/kg), VEN + IACS (VEN, 25 mg/kg + IACS, 7.5 mg/kg) or vehicle (control), and after treatment discontinuation. Mice per group, n = 6. (B) Percentage of hCD45$^+$ cells in the BM and spleen of untreated mice (control) and mice treated with VEN or VEN + IACS, euthanized at day 45. Mice per group, n = 2/3. (C) The Kaplan-Meier analysis of OS of

Additionally, we tested VEN in combination with IACS in a preclinical setting mimicking a relapse event. In detail, when blast percentage in PDX31 reached 40%, we applied an optimized 5-day induction cycle of chemotherapy (cytarabine and doxorubicin).[46] Mice underwent a substantial reduction of blasts in the PB (hCD45 of <5%), however disease progression occurred with a relapse event 43 days after AML onset (Figure 7F). At relapse, mice were randomized and treated with VEN or VEN + IACS. All treated animals reached a second remission. Notably, 10 days after treatment discontinuation, we observed a second relapse event in VEN-treated animals, whereas mice receiving the combined mitochondrial targeting remained in remission (Figure 7G). Considering that IACS development was discontinued due to toxicity reported in a recently closed clinical trial,[47] and the herein documented potential of adding a mitochondrial targeting to VEN, we preliminarily evaluated an alternative compound, atovaquone, a mitochondrial complex III inhibitor currently in use in a clinical trial (ClinicalTrials.gov identifier: NCT03568994).[48] We uncovered its efficacy in pAML samples in vitro, to the same extent as IACS, when in combination with VEN (supplemental Figure 5A).

Because PDX35 model was resistant to VEN plus IACS and AML quickly progressed after treatment discontinuation (66% hCD45$^+$ cells in the PB at day 35; Figure 7A), we attempted to reverse PDX35 resistance by performing a triplet regimen, adding lercanidipine, an agent that we previously used to target the MSCs resident in the leukemic niche (AML-MSCs),[33] to VEN + IACS. This strategy resulted in decreased disease burden in the PB ($P <$ .0001; Figure 7H) and prolonged animal survival ($P < .05$; Figure 7I; supplemental Figure 4E), demonstrating that simultaneous blast-stromal (seed-soil) targeting could be an effective strategy to optimize treatments, particularly in resistant AML. Moreover, because patients with resistant *KMT2A*-r AML are currently treated with VEN combined with AZA or with menin inhibitors (eg, SNDX-5613), we asked whether IACS could enhance the efficacy of these drugs. Briefly, VEN + IACS + AZA or VEN + IACS + SNDX5613 triplets were tested in ex vivo *KMT2A*-r pAML samples. Results highlighted additive effects of mitochondrial targeting when combined with BCL-2 inhibitors and DNA hypomethylating agents, whereas the addition of the menin inhibitor did not provide additional benefit (supplemental Figure 5B-C).

Discussion

The development of innovative therapeutic strategies remains a critical challenge in pAML management.[4] We established a panel of PDX models achieving successful engraftment, particularly for high-risk pAML subtypes. We validated models' similarity to the original AML and found that NSG mice provide an environment that allows pAML cell engraftment and proliferation while preserving their immunophenotype, genetic profile, and self-renewal capacity. Our findings demonstrated that PDXs represent highly efficient in vivo "bioreactors" for the expansion of primary pAML cells, offering a powerful platform for preclinical studies.

We evaluated PDX models' robustness through a comprehensive analysis of pAML mutational profiles. Our data demonstrate the presence of the AML founder clone in murine hosts, despite adaptation to a novel microenvironment. We found that pAML followed a linear model of clonal evolution,[49] with engrafted cells being part of the founder clone and potentially acquiring additional mutations that may enhance tumor fitness. These observations highlight the clinical value of PDX models in capturing the core and the complex genomic landscape of pAML, providing critical insights into genomic factors affecting AML course and supporting ongoing efforts to dissect the clonal architecture of the disease at both diagnosis and relapse.[50] In line with these findings, PDXs emerge as crucial for developing precise, patient-tailored interventions. However, a significant challenge persists in determining the functional and prognostic significance of newly discovered variants. In this study, we identified novel mutated genes whose role will be further explored. Of note, variants in *AXIN1*, *AFF3*, and *FAT1* genes, implicated in Wnt/β-catenin signaling,[51] gave us the opportunity to test ICG-001 as a promising pharmacological treatment. Our results support further investigation of this agent for pAML.

Given the early stage of genomic targeting approaches, we primarily focused our investigation on deregulated pathways to select novel therapeutic interventions for preclinical validation. We selected VEN, a BCL-2 inhibitor, which is one of the most effective targeted drugs currently in use for acute leukemia[38,52] and has great potential to quickly advance in clinic as part of novel combination strategies. However, after VEN treatment, the acquisition of *BCL-2* mutations (as observed for *MEN1* mutations when using menin inhibitors[19]) in parallel with the upregulation of different prosurvival BCL-2 family members, has emerged as a factor resulting in acquired resistance to VEN[20,21,53] and has prompted researchers to identify novel combinations with VEN to limit the development of resistance. Thus, because our models showed *KMT2A*-r pAML relying on aberrant mitochondrial signatures, we combined VEN with IACS to target OXPHOS. The superior efficacy of the combination, previously reported also by Bosc et al,[54] unveiled a strong mitochondrial dependence in *KMT2A*-r AML, supporting further testing of drugs targeting mitochondria, considering IACS withdrawal due to toxicity identified in a recently

Figure 7 (continued) control mice and mice treated with VEN or VEN + IACS. Survival analysis is relative to PDX31 and PDX43. Control mice, n = 6; VEN-treated mice, n = 5; VEN + IACS–treated mice, n = 6. (D) Monitoring of hCD45$^+$ AML cell percentage in the PB of PDX31 during treatment with chemotherapy (Ara-C, 12.5 mg/kg), VEN (25 mg/kg), VEN + IACS (VEN, 25 mg/kg + IACS, 7.5 mg/kg), or vehicle (control), and after treatment discontinuation. Mice per group, n = 6. (E) The Kaplan-Meier analysis of OS of control mice, mice treated with VEN or VEN + IACS, compared with animal treated with Ara-C. Survival analysis is relative to PDX31. Mice, n = 3 per group; log rank Mantel-Cox test. (F) Monitoring of hCD45$^+$ AML cell percentage in the PB of PDX35 treated with VEN (25 mg/kg), VEN + IACS (VEN, 2.5 mg/kg + IACS, 7.5 mg/kg), VEN + IACS + LERCA (VEN, 25 mg/kg + IACS, 7.5 mg/kg + LERCA, 1.5 mg/kg), or vehicle (control). Mice per group, n = 4 to 5. (G) OS was assessed by Kaplan-Meier analysis in control mice (n = 3) and in mice treated with VEN (n = 3), VEN + IACS (n = 4), or VEN + IACS + LERCA (n = 4). (H) Percentage of hCD45$^+$ AML cells in the PB of PDX31 treated with chemotherapy agents (Ara-C, 50 mg/kg and doxorubicin, 1.5 mg/kg). AML complete remission and AML relapse event in treated mice are shown by the purple line (day 12 and day 43, respectively). (I) Monitoring of hCD45$^+$ AML cells in PB of PDX31 treated at relapse (shown in panel F, day 43) with VEN, VEN + IACS) during treatment (2 weeks) and after treatment discontinuation. All data are presented as mean ± SEM. *$P < .05$; **$P < .01$; ***$P < .001$; ****$P < .0001$. Ara-C, cytarabine; LERCA, lercanidipine; OS, overall survival.

closed trial.[47] In support, we preliminary tested atovaquone, which inhibits complex III of the mitochondrial respiratory chain, and showed that, in combination with VEN, it successfully targets pAML in vitro. Atovaquone, recently reported to be well tolerated in a pAML cohort,[48] is currently under evaluation in a phase 1 trial for children and young adults (ClinicalTrials.gov identifier: NCT03568994), introducing a potential use of this drug in this context. Additionally, we proposed a multimodal targeting approach that integrates agents affecting blasts viability with lercanidipine, which acts on stromal cells, aiming to disrupt both intrinsic and extrinsic factors supporting leukemic cell survival and proliferation.[33] "Seed-and-soil" targeting boosted antileukemic drug efficacy in reducing AML progression, suggesting that this may be relevant, especially for refractory AML. Considering that triplet regimens are currently under investigation for patients with mutations in signaling pathway genes, such as *IDH1-2* or *FLT3*[55,56], our microenvironment-directed strategy represents a novel and promising therapeutic avenue in combination with new targeted drugs, as well as the mitochondrial targeting with DNA-hypomethylating agents and VEN.

In conclusion, our study substantiates the pivotal role of PDX models to prioritize druggable AML traits and paves the way for more precise targeted, treatment strategies. The predictive power of PDXs has the potential to significantly accelerate the drug development process by enabling early identification of effective treatments. This could reduce both time and resources needed for clinical trial design, while increasing the likelihood of clinical success, bridging the gap between preclinical findings and real-world clinical outcomes. Although we are aware that PDX models have certain limitations, such as the lengthy timeline required for their generation, which hinders their use in real-time clinical decision-making, and the absence of an immune system, which may obscure significant effects on therapy response, we acknowledge their continued value in preclinical research to ultimately reshape therapeutic strategies and improve precision medicine in pAML treatment.

Acknowledgments

The authors thank the staff of Division of Pediatric Hematology, Oncology and Stem Cell Transplant, Women's and Children's Health Department for diagnostic activity and biobanking (Pediatric Oncohematology BioBank), in particular K. Polato for biological samples management and B. Michielotto for immunophenotypic flow cytometry analysis. They are grateful to Associazione Italiana di Ematologia e Oncologia Pediatrica centers at which children with acute myeloid leukemia were diagnosed and treated. They thank V. Barbieri for his technical support in the mouse facility and E. Campodoni, who contributed to 3-dimensional scaffold synthesis.

This work was supported by grants from the Fondazione Associazione Italiana Ricerca sul Cancro (AIRC; IG grant 20562 [M.P.]), the Associazione Italiana contro le leucemie-linfomi e mieloma (AIL-Treviso [M.P.]), the Fondazione Cariparo (17/04 [M.P.] and 12/20 [S.B.]), the Istituto di Ricerca Pediatrica-Fondazione Città della Speranza (IRP CoG 21/06 [M.P.]), the Fondazione JUST Italia 2023 (M.P.), and Ministero dell'Istruzione, dell'Università e della Ricerca (MIUR) – Progetti di Rilevante Interesse Nazionale 20 (PRIN20) (M.P. and F.L.). M.B. was supported by an AIRC fellowship in Italy.

Authorship

Contribution: A.D.R. was responsible for conceptualization, methodology, data curation, investigation, validation, formal analysis, visualization, and writing the original draft, reviewing, and editing the manuscript; A. Peloso was responsible for the methodology, software, formal analysis, visualization, and data curation; G.L. was responsible for the methodology and investigation; M.B. was responsible for the methodology, investigation, and formal analysis; V.I. was responsible for the software and formal analysis; B.B. and M.S. were responsible for the methodology; S.C. was responsible for the methodology, and reviewing and editing of the manuscript; S.B. was responsible for methodology, software, formal analysis, data curation, reviewing and editing of the manuscript, and funding acquisition; A.R. and A. Pession provided resources, and reviewed and edited the manuscript; F.L. provided resources, reviewed and edited the manuscript, and acquired funding; C.T. supervised the study, and reviewed and edited the manuscript; M.P. was responsible for conceptualization, data curation, project administration, funding acquisition, resources, supervision, and writing the original draft, reviewing, and editing the manuscript.

Conflict-of-interest disclosure: The authors declare no competing financial interests.

ORCID profiles: A.P., 0009-0000-4143-8867; V.I., 0000-0002-8854-3821; S.B., 0000-0001-7677-7084; F.L., 0000-0002-7976-3654; M.P., 0000-0002-4793-5263.

Correspondence: Martina Pigazzi, Department of Women's and Children's Health, University of Padova, Via Giustiniani 3, 35128 Padua, Italy; email: martina.pigazzi@unipd.it.

References

1. Locatelli F, Buldini B, Pigazzi M, et al. Final results of the AIEOP (Associazione Italiana Ematologia/Oncologia Pediatrica) AML 2013 prospective randomized trial in childhood acute myeloid leukemia (AML). *Blood*. 2023;142(suppl 1):728.
2. Rasche M, Zimmermann M, Steidel E, et al. Survival following relapse in children with acute myeloid leukemia: a report from AML-BFM and COG. *Cancers (Basel)*. 2021;13(10):2336.
3. Neel D, Shulman DS, DuBois SG, DuBois SG. Timing of first-in-child trials of FDA-approved oncology drugs. *Eur J Cancer*. 2019;112:49-56.
4. Brivio E, Baruchel A, Beishuizen A, et al. Targeted inhibitors and antibody immunotherapies: novel therapies for paediatric leukaemia and lymphoma. *Eur J Cancer*. 2022;164:1-17.

5. del Bufalo F, Becilli M, Rosignoli C, et al. Allogeneic, donor-derived, second-generation, CD19-CAR-T cell for the treatment of pediatric relapsed/refractory BCP-ALL. *Blood*. 2023;142(2):146-157.
6. Caruso S, De Angelis B, Del Bufalo F, et al. Safe and effective off-the-shelf immunotherapy based on CAR.CD123-NK cells for the treatment of acute myeloid leukaemia. *J Hematol Oncol*. 2022;15(1):163.
7. Pigazzi M, Marini O, Porcù E, et al. Preclinical development of a CAR-T cell approach targeting the CD84 antigen associated to pediatric acute myeloid leukemia. *Blood*. 2022;140(suppl 1):10247-10248.
8. Haubner S, Subklewe M, Sadelain M. Honing CAR T cells to tackle acute myeloid leukemia. *Blood*. 2025;145(11):1113-1125.
9. Bisio V, Zampini M, Tregnago C, et al. NUP98-fusion transcripts characterize different biological entities within acute myeloid leukemia: a report from the AIEOP-AML group. *Leukemia*. 2017;31(4):974-977.
10. Heikamp EB, Henrich JA, Perner F, et al. The menin-MLL1 interaction is a molecular dependency in NUP98 -rearranged AML. *Blood*. 2022;139(6):894-906.
11. Tregnago C, Da Ros A, Porcù E, Simonato M, et al. Thioridazine requires calcium influx to induce MLL-AF6-rearranged AML cell death. *Blood Adv*. 2020;4(18):4417-4429.
12. Yokoyama A, Somervaille TCP, Smith KS, Rozenblatt-Rosen O, Meyerson M, Cleary ML. The menin tumor suppressor protein is an essential oncogenic cofactor for MLL-associated leukemogenesis. *Cell*. 2005;123(2):207-218.
13. Pigazzi M, Masetti R, Bresolin S, et al. MLL partner genes drive distinct gene expression profiles and genomic alterations in pediatric acute myeloid leukemia: an AIEOP study. *Leukemia*. 2011;25(3):560-563.
14. Juul-Dam KL, Shukla NN, Cooper TM, et al. Therapeutic targeting in pediatric acute myeloid leukemia with aberrant HOX/MEIS1 expression. *Eur J Med Genet*. 2023;66(12):104869.
15. Atar D, Ruoff L, Mast AS, et al. Rational combinatorial targeting by adapter CAR-T-cells (AdCAR-T) prevents antigen escape in acute myeloid leukemia. *Leukemia*. 2024;38(10):2183-2195.
16. Tang T, Le Q, Castro S, et al. Targeting FOLR1 in high-risk CBF2AT3-GLIS2 pediatric AML with STRO-002 FOLR1–antibody-drug conjugate. *Blood Adv*. 2022;6(22):5933-5937.
17. Bolouri H, Farrar JE, Triche T, et al. The molecular landscape of pediatric acute myeloid leukemia reveals recurrent structural alterations and age-specific mutational interactions. *Nat Med*. 2018;24(1):103-112.
18. Kantarjian H, Borthakur G, Daver N, et al. Current status and research directions in acute myeloid leukemia. *Blood Cancer J*. 2024;14(1):163.
19. Perner F, Stein EM, Wenge D, et al. MEN1 mutations mediate clinical resistance to menin inhibition. *Nature*. 2023;615(7954):913-919.
20. Thomalla D, Beckmann L, Grimm C, et al. Deregulation and epigenetic modification of BCL2-family genes cause resistance to venetoclax in hematologic malignancies. *Blood*. 2022;140(20):2113-2126.
21. Tausch E, Close W, Dolnik A, et al. Venetoclax resistance and acquired *BCL2* mutations in chronic lymphocytic leukemia. *Haematologica*. 2019;104(9):e434-e437.
22. Jin H, Wang L, Bernards R. Rational combinations of targeted cancer therapies: background, advances and challenges. *Nat Rev Drug Discov*. 2023;22(3):213-234.
23. Sandén C, Lilljebjörn H, Orsmark Pietras C, et al. Clonal competition within complex evolutionary hierarchies shapes AML over time. *Nat Commun*. 2020;11(1):579-10.
24. Kawashima N, Ishikawa Y, Kim JH, et al. Comparison of clonal architecture between primary and immunodeficient mouse-engrafted acute myeloid leukemia cells. *Nat Commun*. 2022;13(1):1624.
25. Belderbos ME, Koster T, Ausema B, et al. Clonal selection and asymmetric distribution of human leukemia in murine xenografts revealed by cellular barcoding. *Blood*. 2017;129(24):3210-3220.
26. Liu Y, Wu W, Cai C, Zhang H, Shen H, Han Y. Patient-derived xenograft models in cancer therapy: technologies and applications. *Signal Transduct Target Ther*. 2023;8(1):160.
27. Stevens AM, Terrell M, Rashid R, et al. Addressing a pre-clinical pipeline gap: development of the pediatric acute myeloid leukemia patient-derived xenograft program at Texas Children's Hospital at Baylor College of Medicine. *Biomedicines*. 2024;12(2):394.
28. Wunderlich M, Chen J, Sexton C, et al. PDX models of relapsed pediatric AML preserve global gene expression patterns and reveal therapeutic targets. *bioRxiv*. Preprint posted online 1 February 2022. https://doi.org/10.1101/2022.01.31.478534
29. Rogojina A, Klesse LJ, Butler E, et al. Comprehensive characterization of patient-derived xenograft models of pediatric leukemia. *iScience*. 2023;26(11):108171.
30. Pession A, Masetti R, Rizzari C, et al. Results of the AIEOP AML 2002/01 multicenter prospective trial for the treatment of children with acute myeloid leukemia. *Blood*. 2013;122(2):170-178.
31. Benetton M, Merli P, Walter C, et al. Molecular measurable residual disease assessment before hematopoietic stem cell transplantation in pediatric acute myeloid leukemia patients: a retrospective study by the I-BFM Study Group. *Biomedicines*. 2022;10(7):1530.
32. Buldini B, Rizzati F, Masetti R, et al. Prognostic significance of flow-cytometry evaluation of minimal residual disease in children with acute myeloid leukaemia treated according to the AIEOP-AML 2002/01 study protocol. *Br J Haematol*. 2017;177(1):116-126.

33. Borella G, Da Ros A, Borile G, et al. Targeting the plasticity of mesenchymal stromal cells to reroute the course of acute myeloid leukemia. *Blood*. 2021;138(7):557-570.
34. Her Z, Su K, Yong M, et al. An improved pre-clinical patient-derived liquid xenograft mouse model for acute myeloid leukemia. *J Hematol Oncol*. 2017;10(1):162.
35. Papaemmanuil E, Gerstung M, Bullinger L, et al. Genomic classification and prognosis in acute myeloid leukemia. *N Engl J Med*. 2016;374(23):2209-2221.
36. Tampieri A, Sandri M, Landi E, et al. Design of graded biomimetic osteochondral composite scaffolds. *Biomaterials*. 2008;29(26):3539-3546.
37. Konopleva M, Pollyea DA, Potluri J, et al. Efficacy and biological correlates of response in a phase II study of venetoclax monotherapy in patients with acute myelogenous leukemia. *Cancer Discov*. 2016;6(10):1106-1117.
38. Masetti R, Baccelli F, Leardini D, Locatelli F. Venetoclax: a new player in the treatment of children with high-risk myeloid malignancies? *Blood Adv*. 2024;8(13):3583-3595.
39. Shukla N, Wetmore C, O'Brien MM, et al. Final report of phase 1 study of the DOT1L inhibitor, pinometostat (EPZ-5676), in children with relapsed or refractory MLL-r acute leukemia. *Blood*. 2016;128(22):2780.
40. Bai H, Zhang SQ, Lei H, Wang F, Ma M, Xin M. Menin-MLL protein-protein interaction inhibitors: a patent review (2014–2021). *Expert Opin Ther Pat*. 2022;32(5):507-522.
41. Aveic S, Viola G, Accordi B, et al. Targeting BAG-1: a novel strategy to increase drug efficacy in acute myeloid leukemia. *Exp Hematol*. 2015;43(3):180-190.e6.
42. Benito JM, Godfrey L, Kojima K, et al. MLL-rearranged acute lymphoblastic leukemias activate BCL-2 through H3K79 methylation and are sensitive to the BCL-2-specific antagonist ABT-199. *Cell Rep*. 2015;13(12):2715-2727.
43. Ball BJ, Arslan S, Koller P, et al. Clinical experience with venetoclax and hypomethylating agents (HMA) in patients with newly diagnosed and relapsed or refractory KMT2A-rearranged acute myeloid leukemia (AML). *Leuk Lymphoma*. 2022;63(13):3232-3236.
44. Molina JR, Sun Y, Protopopova M, et al. An inhibitor of oxidative phosphorylation exploits cancer vulnerability. *Nat Med*. 2018;24(7):1036-1046.
45. Slinker BK. The statistics of synergism. *J Mol Cell Cardiol*. 1998;30(4):723-731.
46. Wunderlich M, Mizukawa B, Chou FS, et al. AML cells are differentially sensitive to chemotherapy treatment in a human xenograft model. *Blood*. 2013;121(12):e90-e97.
47. Yap TA, Daver N, Mahendra M, et al. Complex I inhibitor of oxidative phosphorylation in advanced solid tumors and acute myeloid leukemia: phase I trials. *Nat Med*. 2023;29(1):115-126.
48. Stevens AM, Schafer ES, Li M, et al. Repurposing atovaquone as a therapeutic against acute myeloid leukemia (AML): combination with conventional chemotherapy is feasible and well tolerated. *Cancers (Basel)*. 2023;15(4):1344.
49. Vosberg S, Greif PA. Clonal evolution of acute myeloid leukemia from diagnosis to relapse. *Genes Chromosomes Cancer*. 2019;58(12):839-849.
50. Farrar JE, Schuback HL, Ries RE, et al. Genomic profiling of pediatric acute myeloid leukemia reveals a changing mutational landscape from disease diagnosis to relapse. *Cancer Res*. 2016;76(8):2197-2205.
51. Wang Y, Krivtsov A, Goessling W, et al. The wnt/β-catenin pathway is required for the development of leukemia stem cells in AML. *Science (1979)*. 2010;327(5973):1650-1653.
52. Guerra VA, DiNardo C, Konopleva M. Venetoclax-based therapies for acute myeloid leukemia. *Best Pract Res Clin Haematol*. 2019;32(2):145-153.
53. Ong F, Kim K, Konopleva MY. Venetoclax resistance: mechanistic insights and future strategies. *Cancer Drug Resist*. 2022;5(2):380-400.
54. Bosc C, Saland E, Bousard A, et al. Mitochondrial inhibitors circumvent adaptive resistance to venetoclax and cytarabine combination therapy in acute myeloid leukemia. *Nat Cancer*. 2021;2(11):1204-1223.
55. Liberatore C, Di Ianni M. Novel approaches to treatment of acute myeloid leukemia relapse post allogeneic stem cell transplantation. *Int J Mol Sci*. 2023;24(19):15019.
56. Bewersdorf JP, Shallis RM, Derkach A, et al. Efficacy of FLT3 and IDH1/2 inhibitors in patients with acute myeloid leukemia previously treated with venetoclax. *Leuk Res*. 2022;122:106942.